# Merged Force Diagrams for Expanded Tension-Compression Design Space in Polyhedral Graphic Statics

Hua CHAI\*, Yao LUa, Yefan ZHIb, Masoud AKBARZADEHb

\* College of Architecture & Environmental Design, California Polytechnic State University 1 Grand Ave, San Luis Obispo, CA 93407, USA huchai@calpoly.edu

<sup>a</sup> College of Architecture & the Built Environment, Thomas Jefferson University, USA <sup>b</sup> Polyhedral Structures Laboratory, Weitzman School of Design, University of Pennsylvania, USA

#### **Abstract**

This paper presents a novel approach to structural form-finding using Polyhedral Graphic Statics (PGS), in which two or more force diagrams are computationally merged to generate new diagrams with complex topologies. Unlike conventional methods that directly construct force diagrams composed of convex, non-intersecting cells, the proposed merging strategy enables the creation of intricate force networks that include zero-volume and intersecting cells. These configurations are difficult to achieve through conventional approaches and more closely reflect real-world external loading scenarios. The resulting force diagrams often yield novel structural forms that feature both tension and compression members in equilibrium. Case studies leveraging the Geometric Degrees of Freedom (GDoF) further demonstrate how a merged form diagram can produce multiple distinct structural configurations, each with different arrangements of tension and compression members. Through a clear force mapping process, the method enables designers to implement strategic material selection, placing tension-optimized materials, such as high-strength cables or fiber composites, in areas experiencing tensile forces, while utilizing compression-resistant materials in zones under pressure loads. This expansion of the PGS design space enables innovative structural solutions for architectural applications that require integrated tension-compression systems, ranging from large-span bridges and canopies to potentially revolutionary vertical structures.

Keywords: Structural form-finding, tension-compression structure, algebraic three-dimensional Graphic Statics, Polyhedral Graphic Statics, merge force diagrams

#### 1. Introduction

The combination of structural logic and geometric form represents a fundamental challenge for designers seeking to create lightweight, efficient structures. Graphic Statics (GS) offers a unique framework for this synthesis, visualizing the relationship between structural forces and corresponding members in the form through reciprocal diagrams (Rankine, 1864; Maxwell, 1864; Culmann, 1864). This approach creates an intuitive process that enables designers to directly manipulate design while maintaining structural integrity through visual rather than purely numerical methods.

Extending GS from two to three dimensions experiences fundamental geometric complexities that are linked to form generation. In three-dimensional Graphic Statics (3DGS), the topology and geometry of force diagrams directly determine the set of realizable structural forms. One of the 3DGS methods is the polyhedron-based approach - Polyhedral Graphic Statics (PGS) (Akbarzadeh, 2016), which generates forms through the geometric manipulation of polyhedral force diagrams constructed from non-intersecting polyhedral cells. However, the ability to create and manipulate self-intersecting force diagrams would significantly expand the range of achievable forms, particularly for mixed force structures, such as tension-compression structures.

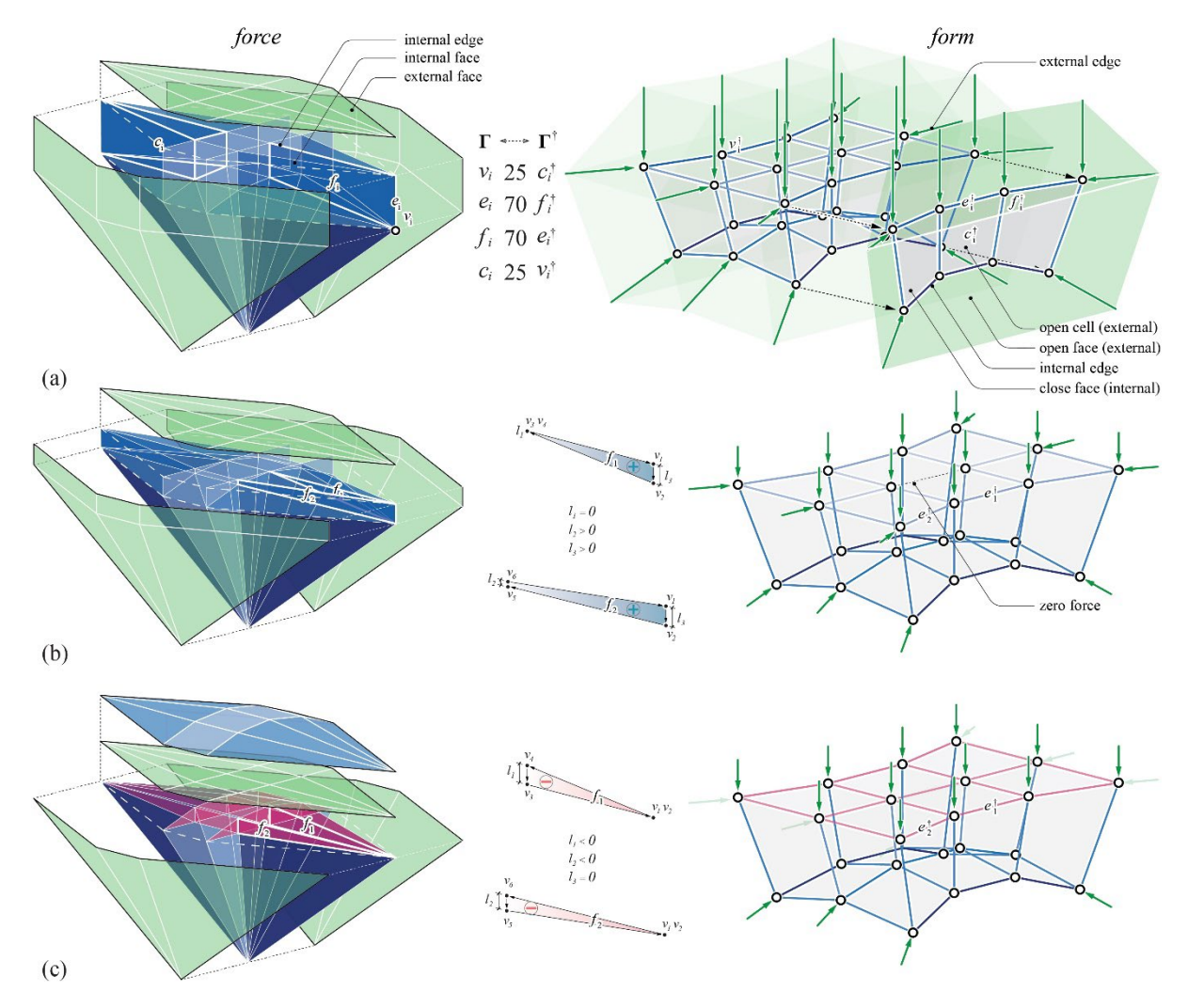


Figure 1. Transformation of compression-only structure to tension-compression through algebraic edge constraints. (a) Initial force diagram with compression cells and corresponding form diagram; (b) intermediate state with edge length constraints -  $l_1 = 0$ ,  $l_2 > 0$ ,  $l_3 > 0$ ; (c) Final configuration with tension cells in upper region and eliminated boundary forces, achieved through complete edge constraint application -  $l_1 < 0$ ,  $l_2 < 0$ ,  $l_3 = 0$ .

Recent developments in algebraic form-finding methods have enabled the rapid generation of forms from geometrically complex force diagrams, including self-intersecting configurations archived through Geometric Degree of Freedom (GDoF), which were previously computationally intractable (Lu et al., 2024). This paper presents a novel geometric method for creating topologically complex force diagrams through diagram merging operations, expanding the design space for computationally generated mixed force forms.

### 1.1. Algebraic 2D/3D graphic statics

The developments in computational methods have addressed the geometric constraints inherent in 3DGS through algebraic formulations. Unlike iterative approaches that require initial feasible configurations, algebraic methods provide exact solutions for reciprocal diagram relationships. The algebraic formulation of GS originated from mathematical descriptions of duality in self-stressed frameworks, establishing the theoretical foundation for computational implementations (Micheletti, 2008). The introduction of linear algebraic systems for reciprocal constraints marked a significant advancement, enabling analytical computation of force distributions from form diagrams through edge vector closure conditions (Van Mele & Block, 2014). This approach computes all internal and external force magnitudes directly from the connectivity and geometry of structural forms. Subsequent developments introduced bidirectional manipulation capabilities, transforming algebraic GS into an interactive design tool (Alic, 2017). This advancement allows real-time synchronization between force and form diagrams, where modifications to either diagram automatically update its reciprocal counterpart, facilitating iterative design exploration in two dimensions.

The three-dimensional extension required fundamental reformulation of algebraic constraints. A comprehensive framework for 3DGS was established using linear systems that enforce coplanarity and closure conditions for polyhedral face vectors (Hablicsek et al., 2019). This method generates all possible reciprocal configurations through closed-form solutions, accepting either force or form diagrams as input. Enhanced formulations incorporated user-specified edge length constraints, providing parametric control over the solution space (Akbarzadeh & Hablicsek, 2020), though vertex positioning remained indirect compared to iterative methods (Nejur & Akbarzadeh, 2021). A quadratic formulation was developed to incorporate face area constraints alongside edge lengths, enabling direct control over force magnitudes through geometric manipulation of polyhedral faces (Akbarzadeh & Hablicsek, 2021). This capability proved particularly valuable for exploring tension-compression structures. However, the quadratic nature increased computational complexity. Recent improvements integrated vertex constraints and enhanced numerical stability while maintaining computational efficiency (Lu et al., 2024). These advances make algebraic methods practical for solving complex polyhedral form-finding problems.

Building on these algebraic advances, the edge constraint formulation enables the transformation of force diagrams to generate structural systems that incorporate tension and compression. Figure 1 demonstrates this capability through the modification of the initial compression-only structure. In the configuration Figure 1(a), the force diagram consists entirely of polyhedral cells oriented to represent compressive forces. The corresponding form diagram shows a structure with uniformly distributed internal forces and external loads at the boundary vertices. Through the application of edge constraints in the algebraic formulation, specific edges in the force diagram can be assigned zero length ( $l_3=0$ ), effectively eliminating their corresponding forces in the form diagram. This operation induces topological changes in the force polyhedra, causing certain faces (for example,  $f_1 & f_2$ ) to flip their orientation, a geometric transformation that corresponds to a reversal in force type from compression to tension. The intermediate state Figure 1(b) shows the initiation of this process, where edge constraints begin to modify the force distribution while maintaining overall equilibrium. The final configuration, Figure 1(c), reveals the complete transformation that the upper portion of the force diagram now contains inverted polyhedra, indicating tensile forces

in the corresponding structural members. Simultaneously, the lateral forces at the upper boundary have been eliminated through the edge constraints. This approach represents the current state-of-the-art for generating mixed-force structures in PGS.

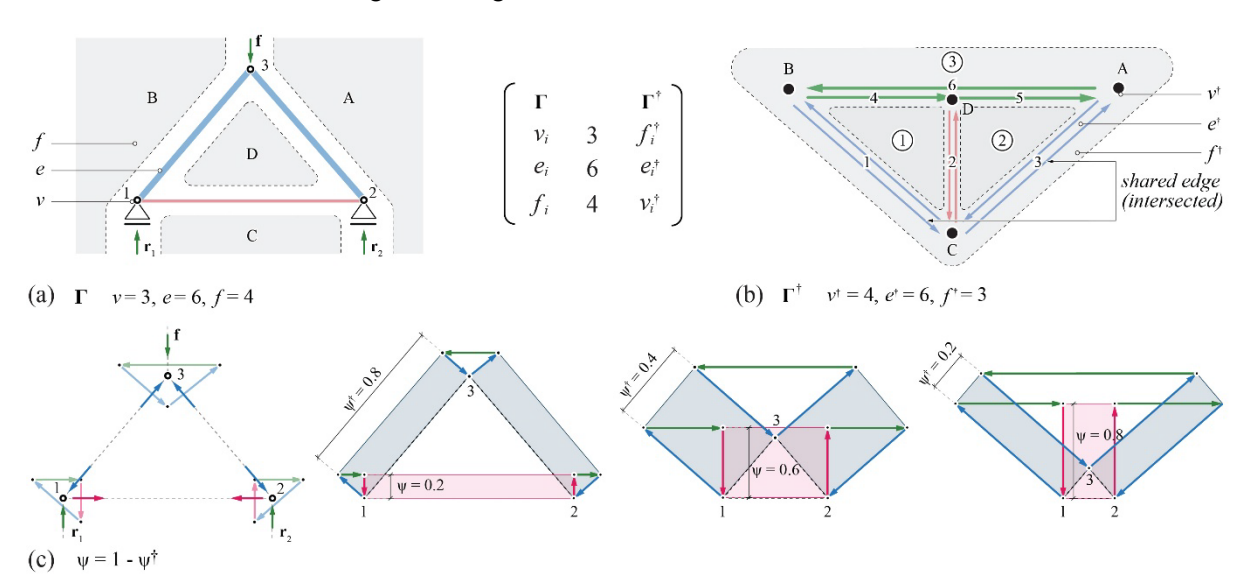


Figure 2. (a) Form diagram; (b) force diagram showing shared edges between adjacent polygons; (c) Minkowski sum transformation demonstrating the geometric transition from form to force diagram.

## 1.2. Problem statement and objectives

While previous approaches to PGS, either iterative or algebraic methods, often constrain designers to begin with non-intersecting convex force polyhedron configurations. The proposed method overcomes this limitation by introducing algorithms for identifying and merging compatible faces between distinct polyhedral force diagrams, thereby enabling the creation of integrated structural systems beyond compression-dominant structures. The merging process follows a rigorous workflow that identifies corresponding faces, then establishes topological consistency when joining the separate diagrams. This includes remapping vertex indices, edge connections, and face definitions to ensure structural coherence in the merged system. The resulting unified polyhedral force diagram maintains equilibrium while expanding the potential design space.

#### 2. Method

This section develops a geometric framework for constructing topologically linked force diagrams of PGS. By introducing controlled merging operations between polyhedral cells, enabling the generation of self-intersecting configurations while maintaining the mathematical validity of the reciprocal relationships. The methodology addresses three critical aspects: first, the identification of geometrically compatible merge candidates within existing force diagrams; second, the execution of topological operations that preserve equilibrium conditions during cell mixing; and third, the resolution of geometric conflicts arising from overlapping polyhedral volumes. This framework leverages the recent advances in algebraic form-finding to compute valid designs from these complex force configurations, establishing a direct computational pipeline from geometric manipulation to form generation.

## 2.1. Geometric principle in two-dimensional graphic statics

The merging methodology begins with two-dimensional force diagrams to establish the fundamental principles before extending to three dimensions. Figure 2 illustrates this process through a simple truss example. The form diagram ( $\Gamma$ ) shows a symmetric truss. The corresponding force diagram ( $\Gamma^{\dagger}$ ) consists of separate polygons for each node: triangle ABC for node three, triangles BCD and ACD for nodes one and two. Each polygon satisfies local equilibrium through vector closure, with edge width proportional to force magnitudes and orientations following the 90-degree rotation convention.

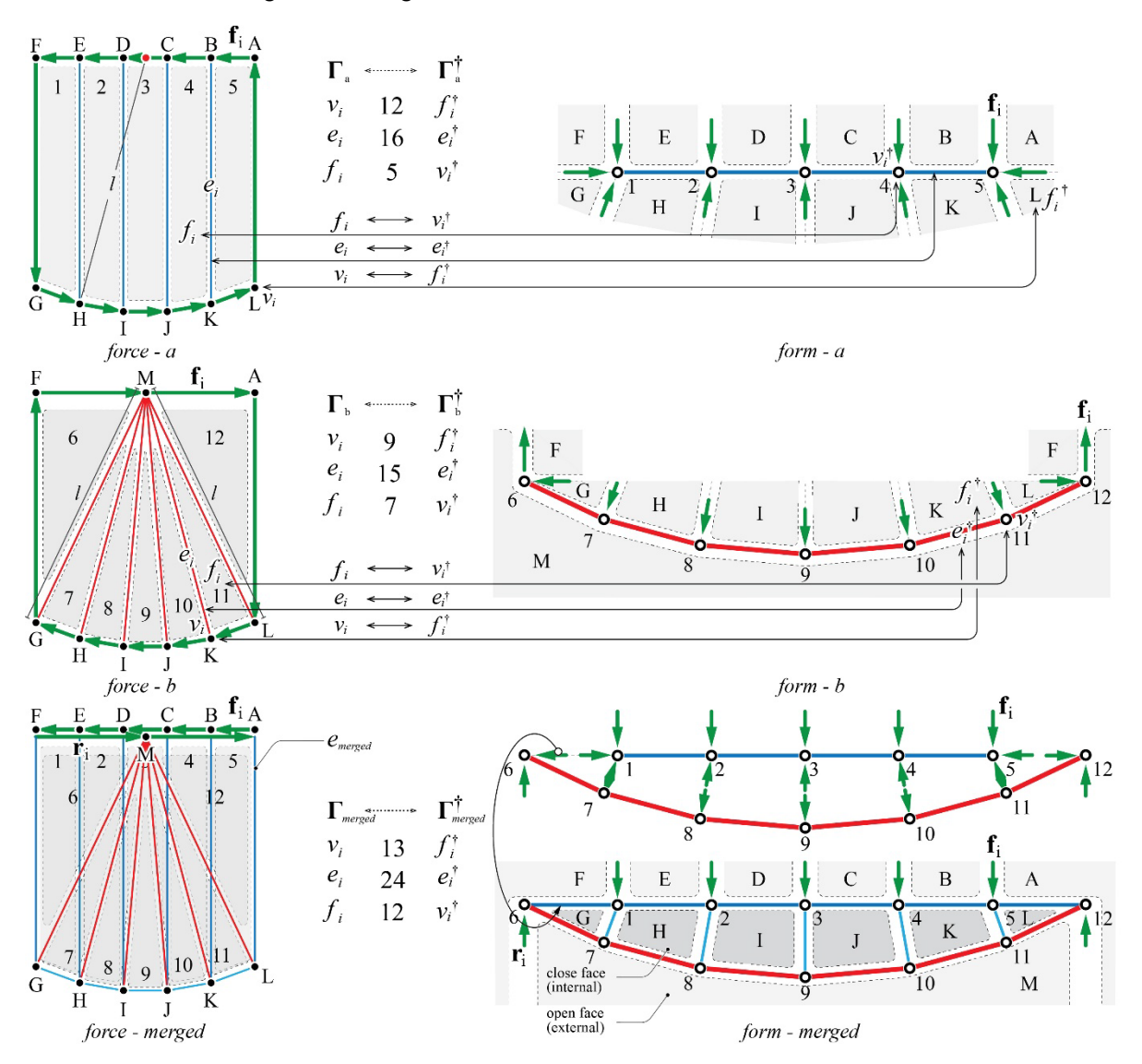


Figure 3. Edge merging operation in 2D graphic statics. Top row: initial compression-only system with trapezoid force polygon and corresponding horizontal member form diagram; middle row: introduction of force and form diagram for tension-only members; bottom row: merged configuration with intersecting force diagram combining compression (blue) and tension (red) members.

The form diagram ( $\Gamma$ ) Figure 2(a) shows a truss configuration with a single applied load and three nodes, supported by two reaction forces  $r_1$  and  $r_2$ . The topology is defined by vertices (v=3), edges (e=6), and faces (f=4). The corresponding force diagram, Figure 2(b), represents the equilibrium state through closed polygons. Here, the dual topology exhibits

 $v^\dagger=4$ ,  $e^\dagger=6$  and  $f^\dagger=3$ , with force polygons arranged such that each closed loop corresponds to equilibrium at a node in the form diagram. The critical aspect of this two-dimensional implementation lies in identifying shared edges between force polygons. In the force diagram Figure 2(b), the shared edges are defined from polygons 1&3 and 2&3, the corresponding edges in the form diagram Figure 2(a) are compressive members connecting node 1&3 and 2&3.

The geometric relationship between form and force diagrams is revealed through the Minkowski sum construction shown in Figure 2(c). This parametric transformation  $\psi=1-\psi^\dagger$  demonstrates how the form diagram morphs into the force diagram through continuous geometric operations. At  $\psi=0.2$ , the diagram shows edges moving toward their perpendicular orientations. The shaded regions indicate the evolving polygon areas, while the blue segments highlight edges that will merge in the final force configuration. This two-dimensional example establishes the fundamental principle that force diagrams naturally contain redundant edges at polygon boundaries, and these shared edges can be merged to create self-intersecting configurations.

### 2.2. Merging operations in two-dimensional force diagrams

Figure 3 illustrates the complete merging process for creating intersecting force diagrams through a more complex example. First, setting up the initial force polygons (force-a) representing a compression-only structure, with its corresponding form diagram showing horizontal structural members. The topological relationship reveals  $v=f^{\dagger}=12$ ,  $e=e^{\dagger}=16$ ,  $f=v^{\dagger}=5$ . Second, creating another set of triangular force polygons (force-b), which share boundary edges with the force-a. This triangular element, centered at vertex M, introduces radial edges that connect to the perimeter vertices. The resulting topology shows reduced counts  $(v=f^{\dagger}=9, e=e^{\dagger}=15, f=v^{\dagger}=7)$ . The corresponding form diagram illustrates how these new force elements generate arc members that introduce potential tension into the previously defined boundary condition of the compression-only system.

The merging operation (force-merged) demonstrates the topological transformation. Shared edges from two force diagrams are identified and merged, creating an intersecting force diagram. This operation increases the topological complexity with  $v=f^\dagger=13$ ,  $e=e^\dagger=24$ ,  $f=v^\dagger=12$ . The merged force diagram consists of two distinct regions: the outer trapezoidal zone (faces  $f_{1-5}$ ), representing compression forces, and the inner triangular zone (faces  $f_{6-12}$ ), representing tension forces. In the resulting form diagram (force-merged), the structural interpretation becomes clear. The first group of members remains in compression, while the diagonal members act in tension, creating a combined structural scheme. The merging process preserves equilibrium at each node while enabling the coexistence of opposing force types within a single diagram. Notably, the merged configuration creates both closed internal faces and open external faces in the form diagram, demonstrating how topological operations on force diagrams directly influence the topology.

## 2.3. Computational merging operations in PGS

While the two-dimensional examples demonstrate the conceptual foundation of merging operations, implementing these principles in three-dimensional PGS requires addressing fundamental differences in topology and geometry. In 3D, shared edges become shared faces, and force polygons become force polyhedra. This section presents a computational framework

that handles these complexities through three integrated phases: geometric validation, topological reconstruction, and algebraic approach.

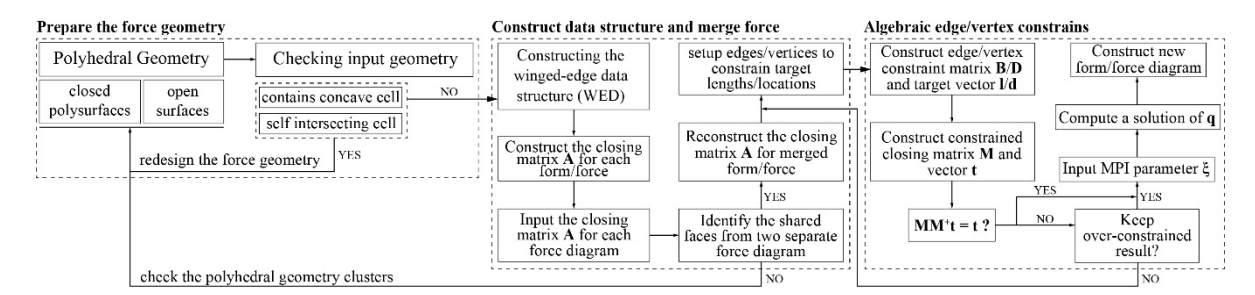


Figure 4. Computational workflow for generating mixed force structures. Three-phase process: (1) Force geometry preparation with polyhedral validation and geometric checks, (2) Data structure construction using winged-edge format and closing matrix computation, and (3) Algebraic constraints implementation. Decision points ensure geometric validity and constraint satisfaction with feedback loops for redesign when needed.

The workflow (Figure 4) begins with preparing the force geometry, where polyhedral inputs are classified as either closed polysurfaces or open surfaces. Critical geometric validation ensures the viability of merging operations by checking for two specific conditions: the presence of concave cells and self-intersecting cells within the initial configuration. These geometric irregularities must be identified early, as they fundamentally affect the subsequent topological operations. If such conditions are detected, the force geometry requires redesign before proceeding, ensuring that the input polyhedra meet the basic requirements for successful merging.

With valid input geometry established, the workflow proceeds to its core operation: the topological merging of polyhedral cells. First, the Winged-edge Data Structure (WED) is constructed for the input polyhedra, providing the topological framework necessary for identifying and manipulating shared geometric elements. For non-merged configurations, the process directly constructs the closing matrix **A** for each individual force diagram, maintaining separate polyhedral cells. However, when merging is required, the algorithm identifies shared faces between separate force diagrams, the three-dimensional analogue of shared edges in 2D. These shared faces represent locations where polyhedral cells can be topologically fused. The merging operation then reconstructs a unified closing matrix **A** that encompasses the merged configuration, effectively creating a single topological entity from previously separate polyhedra.

The identification of compatible faces forms the foundation of successful merging operations. To establish this compatibility, introduce a similarity metric that evaluates geometric correspondence between candidate interface faces. Let  $f_a \in F_a$  and  $f_b \in F_b$  be candidate interface faces. Then establish compatibility through the evaluation of three primary geometric properties: area correspondence, centroid location, and bounding box vertex projection alignment.

$$\sigma(f_a, f_b) = \frac{\left|A_{f_a} - A_{f_b}\right|}{\max(A_{f_a} A_{f_b})} + \frac{\left||c_{f_a} - c_{f_b}|\right|}{d_{max}} + \delta_{VP}(f_a, f_b)$$
(1)

This equation defines a similarity metric  $\sigma(f_a,f_b)$  that quantifies how well two faces  $f_a$  and  $f_b$  from different force polyhedron match each other as potential interface faces for merging. Lower values of  $\sigma$  indicate greater similarity between faces, where  $A_{f_i}$  represents face area,  $c_{f_i}$  denotes face centroid,  $d_{max}$  is the maximum characteristic dimension of the system,  $\delta_{VP}(f_a,f_b)$  represents the vertex projection alignment metric that compares the two faces bounding box along the coordinate axes. This could be defined as:

$$\delta_{VP}(f_a, f_b) = \frac{1}{3} \sum_{i \in x, y, z} \frac{|\min_i(f_a) - \min_i(f_b)| + |\max_i(f_a) - \max_i(f_b)|}{\max(\operatorname{range}_i(f_a), \operatorname{range}_i(f_b))} \tag{2}$$

This vertex projection alignment metric compares the spatial extents of the two faces along each coordinate axis, where  $\min_i$  and  $\max_i$  represent the minimum and maximum coordinates, and  $range_i$  denotes the coordinate range along axis i. Compatible faces are identified when  $\sigma(f_a,f_b)<\varepsilon$ , where  $\varepsilon$  is a user-defined tolerance. Once faces are identified, a consistent indexing system must be established to ensure topological coherence in the merged structure. This requires a mapping function  $\phi\colon V_a\cup E_a\cup F_a\cup C_a\to V_b\cup E_b\cup F_b\cup C_b$  that satisfies reciprocal constraints between form and force diagrams. Once the merging faces are identified, all elements (vertices, edges, and faces) must be re-indexed to create a coherent unified structure:

$$\begin{cases}
\text{Force - 1} : v_0 \mapsto v_n, e_1 \mapsto e_n, f_1 \mapsto f_n \\
\text{Force - 2} : v_{n+1} \mapsto v_m, e_{n+1} \mapsto e_m, f_{n+1} \mapsto f_m
\end{cases}$$
(3)

Following face identification, the merging process requires re-indexing to create a unified topological structure. This re-indexing must preserve the individual identity of elements while establishing new relationships at the interface. In the vertex re-indexing phase, vertices from the first force diagram retain their original indices from 0 to n, while vertices from the second diagram receive new indices starting from n+1. This creates a continuous vertex indexing scheme where  $v_i^{\rm new}=v_i$  for  $i\in n+1,\dots,n+m$ . This indexing ensures that each vertex in the merged structure has a unique identifier while preserving the original identifiers of the first diagram. The edge re-indexing follows a similar approach to maintaining continuity throughout the unified structure. The face re-indexing requires special handling since two faces (one from each diagram) will be merged. The re-indexing scheme excludes these faces from the individual diagrams. Specifically,  $f_i^{\rm new}=f_i^1$  for all faces in the first diagram except the merging face  $f_i$ , and  $f_i^{\rm new}=f_{i-n_f+1}^2$  for all faces in the second diagram except the merging face  $f_j$ . This careful exclusion and renumbering ensures that the merged structure contains exactly the right number of faces without duplication at the interface.

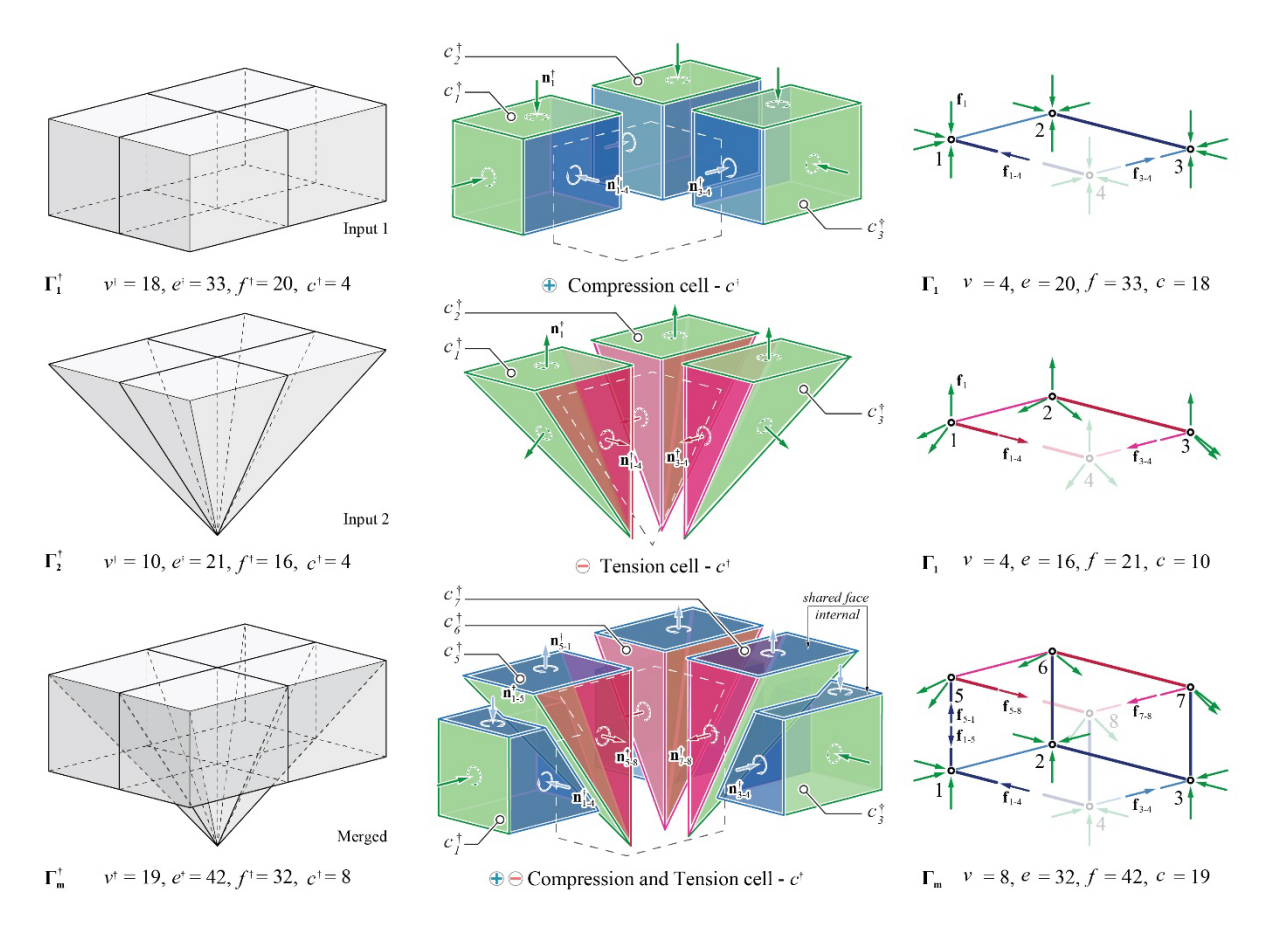


Figure 5. Three-dimensional polyhedral merging process. Left column: force diagrams showing compression, tension, and merged configuration with topological indices. Middle column: exploded views revealing cell orientations—compression cells (blue), tension cells (red), and interface relationships. Right column: reciprocal form diagrams displaying generated structures with numbered nodes and force vectors.

The merged topology must satisfy both local and global equilibrium conditions, expressed through a hierarchy of constraint equations. These constraints ensure that the merged configuration maintains the fundamental reciprocal relationships of PGS. The final phase applies algebraic constraints to generate valid reciprocal diagrams from the merged force configuration. Users can specify edge lengths, vertex locations, or both, constructing the constraint matrix  ${\bf B}$  and target vector  ${\bf d}$  that define desired geometric properties. The constrained closing matrix  ${\bf M}$  and vector  ${\bf t}$  incorporate these specifications into the algebraic formulation. The topological consistency is maintained through the implementation of linear closing equations. Let  ${\bf C}_{e_{int}\times f_{int}}$  denote the internal edge-face connectivity matrix of the merged force diagram  $\Gamma$ . For each internal face  $f_i^{\dagger}$  in the corresponding form diagram  $\Gamma^{\dagger}$ , the closure constraint can be expressed as:

$$\sum_{j=1}^{e_{int}} \mathbf{C}_{ji} \cdot \mathbf{n}_j \cdot \mathbf{q}_j = \mathbf{0}$$
 (4)

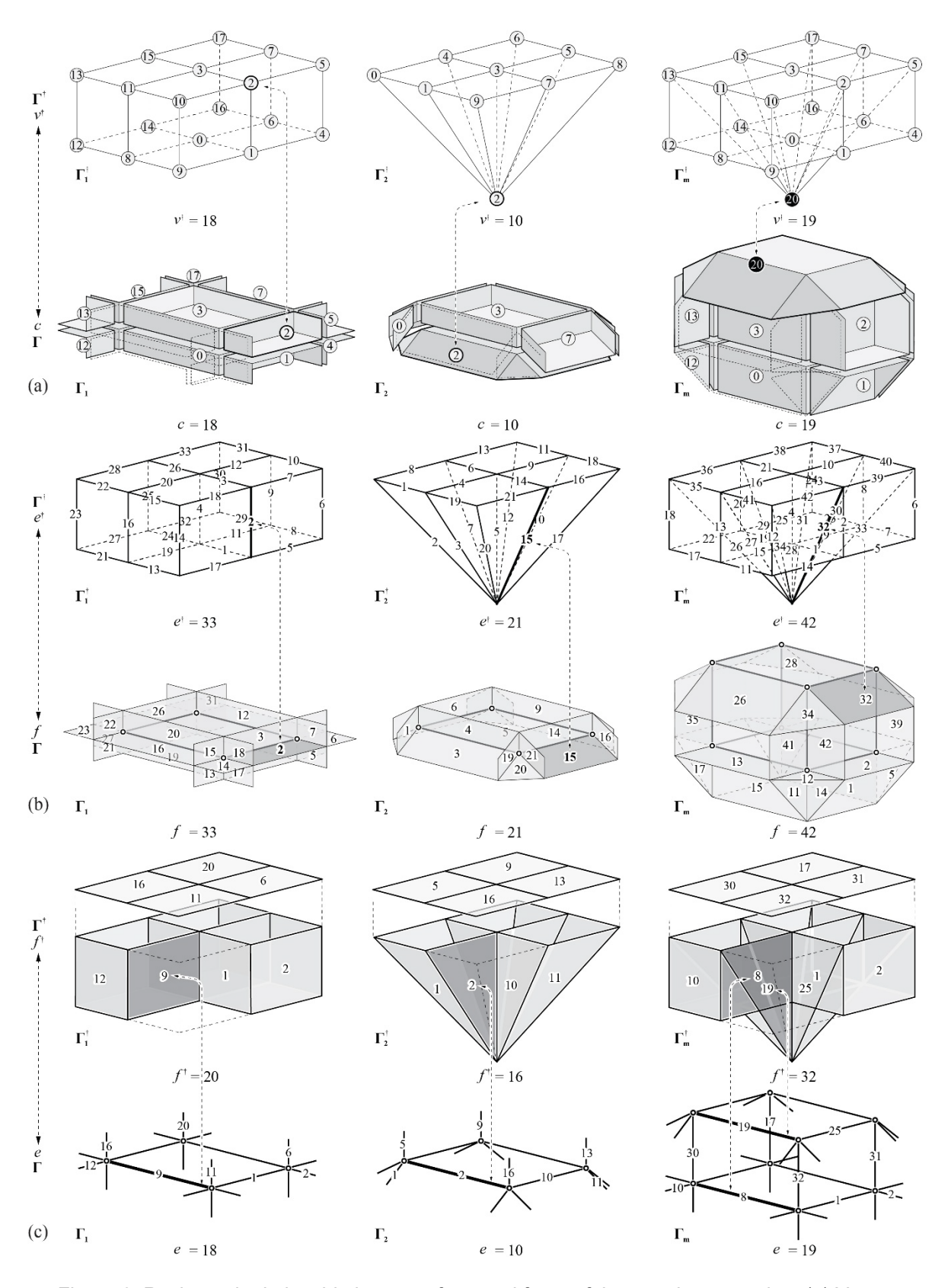


Figure 6. Reciprocal relationship between form and force of the merging operation. (a) Vertex connectivity and labeling schemes for individual and merged re-indexed configurations; (b) edge indexing shows the integration of 33 + 21 edges into 42 unique edges; (c) face labeling with gray-shaded interface faces and corresponding structural diagrams showing force flow patterns in the final hybrid system.

where  $\mathbf{n}_j$  is the unit normal vector of face  $f_j$  in the force diagram, and  $\mathbf{q}_j$  represents the signed length of edge  $e_i^{\dagger}$  in the form diagram.

The reconnection of edges and vertices at the interface follows a rigorous protocol to ensure geometric and topological validity. For each identified interface, establish edge correspondence through normal vector alignment, generating a set of constraint equations that enforce reciprocity:

$$(\mathbf{P}_i \mathbf{n}'_{xi})^T = 0, \quad (\mathbf{P}_i \mathbf{n}'_{vi})^T = 0 \tag{5}$$

where  $\mathbf{P}_i$  is the  $[f_{int} \times f_{int}]$  diagonal matrix that describes the edge-face connectivity for face  $f_i^{\dagger}$ , and  $\mathbf{n}_{xi'}$ ,  $\mathbf{n}_{yi'}$  are the transformed unit directional vectors in the local coordinate system of face  $f_i^{\dagger}$ . The complete constrained closing matrix  $\mathbf{M}$  for the merged system combines closure constraints, edge constraints, and vertex constraints:

$$\mathbf{M} = \begin{pmatrix} \mathbf{A} \\ \mathbf{B} \\ \mathbf{D} \end{pmatrix} \tag{6}$$

where A is the closing matrix, B is the edge constraint matrix, and D is the vertex constraint matrix.

Through this systematic approach, the computational framework transforms separate polyhedral force diagrams into unified, self-intersecting configurations. The method preserves the mathematical rigor of algebraic graphic statics while enabling geometric operations that were previously infeasible.

Building on the computational framework, the practical implementation of polyhedral merging is illustrated through a simplified example that demonstrates the transformation from separate compression and tension systems to a unified structure. Figure 5 presents the complete merging process in three dimensions. The first input  $(\Gamma_1^\dagger)$  consists of a rectangular arrangement of four polyhedral cells representing a compression-only system. Each cell  $(c_i)$  maintains consistent inward-facing normals. The corresponding form diagram  $(\Gamma_1)$  shows a grid-like structural configuration with purely compressive members. The second input introduces a pyramidal force diagram  $(\Gamma_2^\dagger)$ . These cells, shown in red, represent tensile forces with outward-facing normals. The form diagram  $(\Gamma_2)$  reveals a tension-dominated structural system where forces are directed away from the boundary nodes. The merging operation identifies the shared rectangular face at the top of the pyramidal force as the interface between the two force diagrams. This face satisfies the compatibility criteria established in the

computational framework: identical area, coincident centroids, and aligned boundary vertices. The merged configuration  $(\Gamma_m^\dagger)$  creates a self-intersecting force diagram where the tension pyramid is combined with the compression box, yielding a complex topology with  $v^\dagger=19$ ,  $e^\dagger=42$ ,  $f^\dagger=32$ ,  $c^\dagger=8$ . The cells are now classified into two categories: pure compression (  $c_1$  &  $c_2$  &  $c_3$  ), and compression-tension cells (  $c_5$  &  $c_6$  &  $c_7$  ) at the interface. The resulting form diagram (  $\Gamma_m$  ) demonstrates how this topological fusion generates a sophisticated structural system combining horizontal compression members with diagonal tension members, all meeting at integrated nodes that balance both force types.



Figure 7. Structural implementation of the pedestrian bridge derived from merged force diagrams, showing the integration of compression members (white branching network) and tension cables (thin black lines).

Figure 6 provides a detailed visualization of the merging process through decomposition of the topological elements. Row (a) shows the vertex labeling and connectivity, revealing how vertices from both diagrams are preserved and re-indexed according to the merging protocol. The merged configuration shows vertex  $v_2^\dagger$  as the apex of the tension pyramid, now embedded within the compression system and re-indexed as vertex  $v_{20}^\dagger$ . Row (b) illustrates edge indexing, where the original 33 edges from  $\Gamma_1^\dagger$  and 21 edges from  $\Gamma_2^\dagger$  combine and share common edges at the interface, resulting in 42 unique edges in  $\Gamma_m^\dagger$ . Row (c) presents face labeling, with particular attention to the intersected faces that facilitate the topological connection. The reindexing ensures that faces  $f_{1-20}^\dagger$  derive from the compression system, faces  $f_{21-32}^\dagger$  from the tension system, with careful handling of the eliminated duplicate interface

faces. This three-dimensional example demonstrates that the self-intersecting nature of the merged force diagram directly translates to structural configurations where tension and compression elements coexist and interact within the same spatial volume.

## 3. Case Study: Tension-Compression Bridge Design

The practical application of merged force diagrams is demonstrated through the design of a pedestrian bridge that integrates tension and compression elements within a unified structural system (Figure 7). The bridge design utilizes a branch of compression members and a series of cables as tension members, which work in concert to transfer the applied loads to the supports. The force diagram (Figure 8(a)) reveals a complex self-intersecting polyhedral assembly containing 109 cells, 258 faces, 197 edges, and 48 vertices. The global forces after the merged operation are now represented by two layers of green boundary faces, which represent the external forces on the bridge, including both applied loads on the deck surface and reaction forces at the abutments. The rest of the blue and red polyhedral cells encode the internal force distribution, with their orientations indicating compression and tension respectively.

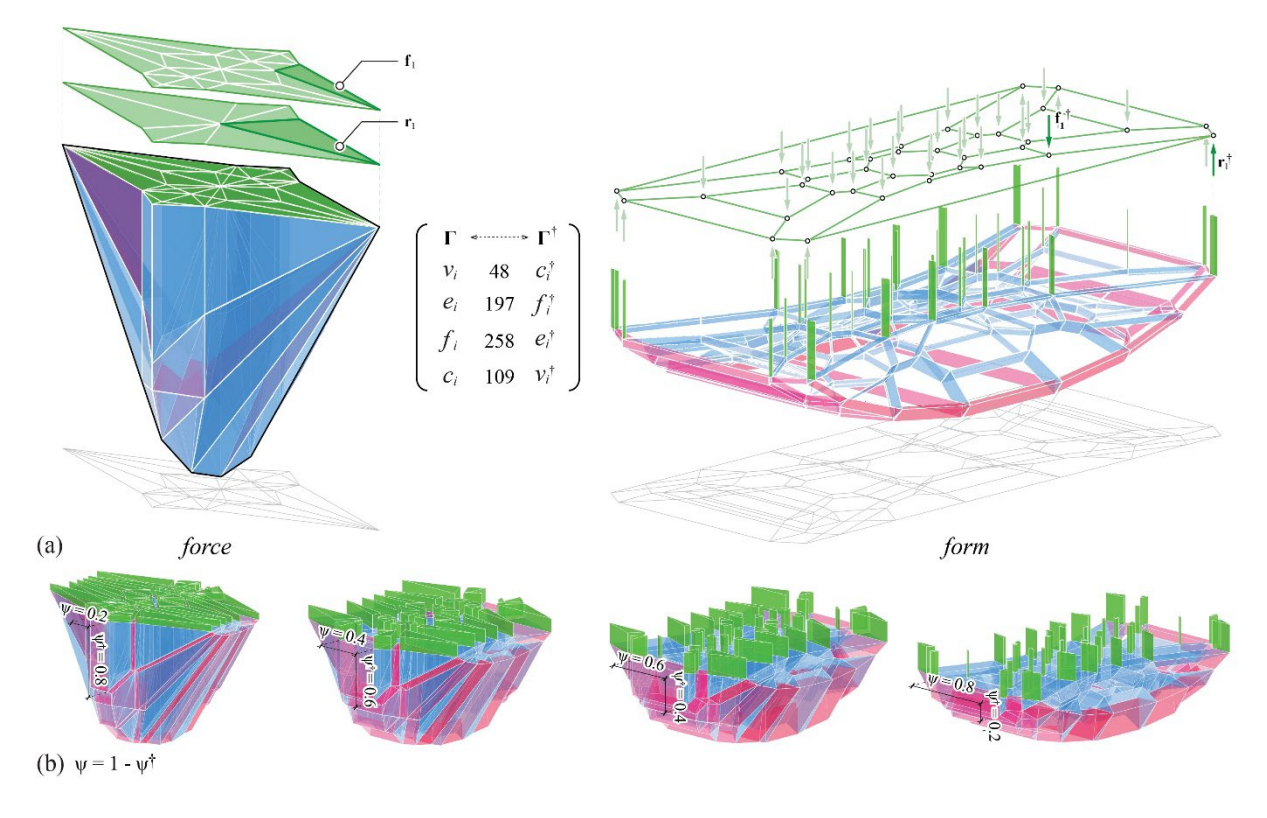


Figure 8. Bridge design case study using merged force diagrams. (a) Force diagram (left) showing merged polyhedral configuration with 109 cells, and corresponding form diagram (right) revealing tension-compression combined structure; (b) Minkowski sum transformation demonstrating parametric evolution from force to form geometry.

The corresponding form diagram (Figure 8(a)) translates this geometric complexity into the structural solution. Green vectors indicate the external force system: downward applied loads distributed across the network and upward reactions at the supports. The structural response manifests through a network of compression struts (derived from blue cells in the force diagram) forming the upper chord, while tension cables create the lower support system. The reciprocal relationship ensures that member sizes are precisely calibrated to their force magnitudes, with cross-sectional areas proportional to the corresponding face areas in the force diagram.

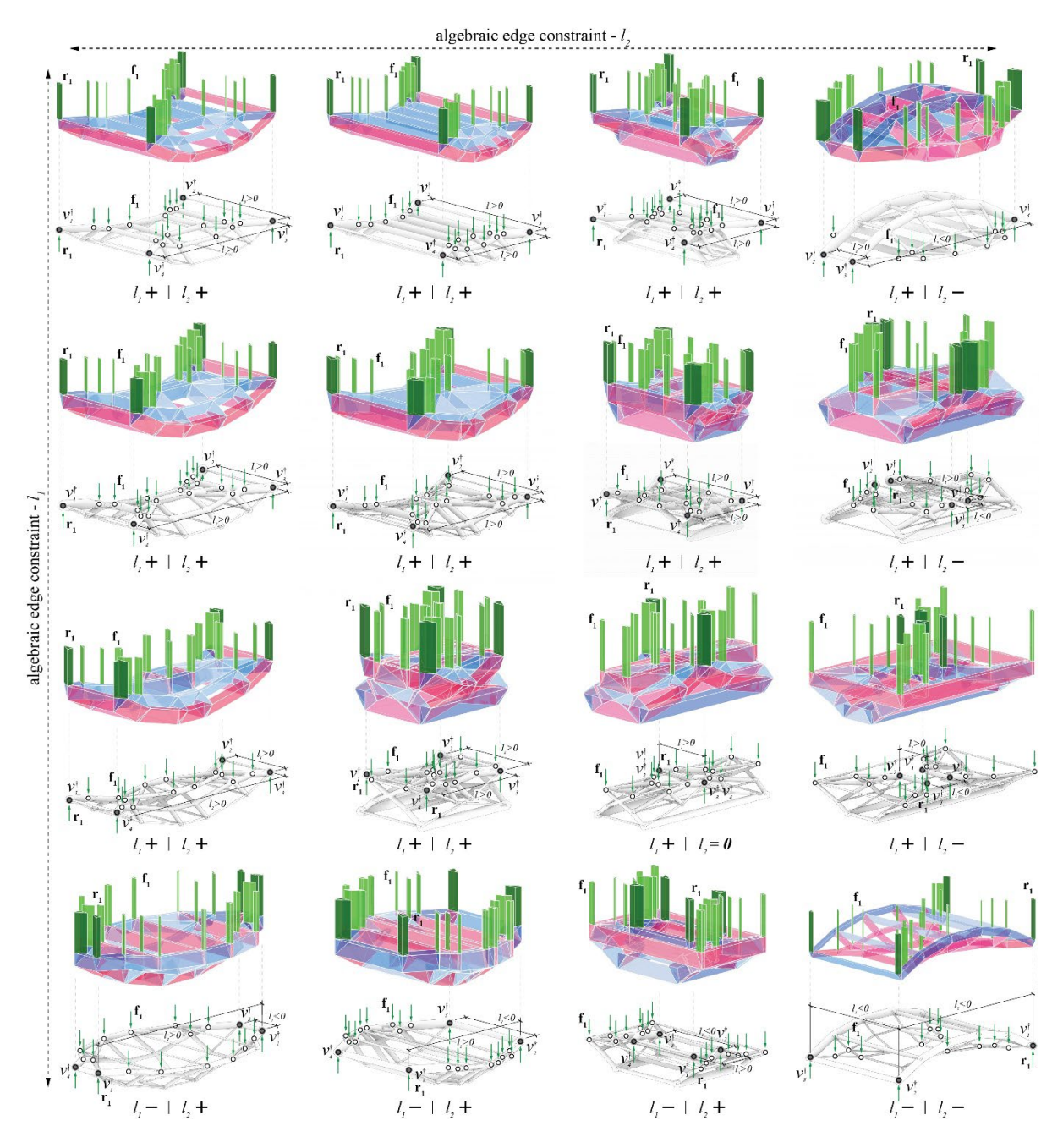


Figure 9. Design exploration through algebraic edge constraints on the merged force diagram. Matrix of 16 variations showing manipulation of edge length  $l_1 \& l_2$  from positive to negative directions, with algebraic relationships governing structural configurations.

The Minkowski sum transformation is now also extended in 3D to present the fundamental reciprocal relationship between the merged force diagram and its corresponding form diagram. Figure 8(b) illustrates this geometric transformation at four stages. At  $\psi=0.2$ , the self-intersecting polyhedral cells begin to differentiate, with blue cells rotating toward becoming compression members while red cells orient to form tension elements. When  $\psi=0.8$ , the reciprocal relationship is fully realized: blue polyhedral cells have transformed into upper compression struts while red cells manifest as lower cables. The continuous transformation demonstrates that despite the geometric complexity of self-intersecting polyhedra, the framework maintains mathematical validity throughout.

### 3.1. Design exploration through algebraic edge constraints

The versatility of the merged force diagram approach is further demonstrated through the application of algebraic edge constraints. Figure 9 presents a comprehensive exploration of the bridge design space, showing how targeted edge length modifications generate fundamentally different structural configurations while maintaining equilibrium. The horizontal progression (left to right) shows variations in edge constraint of  $l_2$  lengths, while the vertical progression (top to bottom) varies the edge constraint  $l_1$ . The signs (+ or -) indicate the edge direction, allowing members to flip their orientation within the force diagram. Tension members are no longer restricted to the bottom of the structure. By manipulating edge lengths and directions, the methodology enables tension elements to occupy any position within the structural system—above, below, or interwoven with compression members. When edge constraints flip from positive to negative, the curved edges in the force diagram can reorient completely, causing members to transition between tension and compression states while relocating their position in space.

This spatial freedom transforms the design possibilities for mixed force structures. In configurations where  $l_2$  assumes negative values, tension cables that traditionally span beneath the deck can migrate upward, creating overhead suspension systems. Similarly, when both  $l_1$  and  $l_2$  are manipulated, tension members can spiral through the structure, occupying diagonal and vertical positions that would be impossible in conventional separated force diagrams. The self-intersecting nature of the merged force diagram is crucial here, as it allows tension and compression zones to overlap and interpenetrate, enabling members to pass through different force regions as they respond to the algebraic constraints. This three-dimensional distribution of opposing force types creates opportunities for alternative structural designs where the traditional

hierarchies of compression-above and tension-below are modified, which can adapt to complex site-specific requirements.



Figure 10. Physical model at 1:25 scale demonstrating the constructability of structures where 3D-printed compression members integrate with tension cables.

The 1:25 scale physical model (Figure 10) validates the constructability of structures derived from merged force diagrams. 3D-printed at 400mm length, the model demonstrates three critical aspects: first, the multi-member nodes successfully resolve the complex intersections where up to six compression members converge, confirming that shared faces in the force diagram translate to viable physical connections. Second, the tension cables thread through the compression network without interference, maintaining the clearances necessary for assembly and prestressing. Third, the integrated system achieves lateral stability through three-dimensional triangulation; the model stands without external support, resisting lateral loads through the spatial distribution of members rather than requiring additional bracing. The fabrication process itself proved straightforward: the compression network was printed as a single continuous piece, eliminating joint weaknesses, while tension cables were post-tensioned through predetermined paths.

#### 4. Discussion and conclusion

This paper has presented a methodology for creating self-intersecting polyhedral force diagrams through topological merging operations, extending the capabilities of PGS beyond the constraint of non-intersecting cells. The computational framework

successfully merges separate force polyhedra by identifying compatible faces, reindexing topological elements, and reconstructing the algebraic closing matrix to maintain equilibrium. Future applications extend to vertical structures where merged force diagrams could revolutionize tower design by enabling tension members to spiral through compression cores at multiple heights, creating hybrid systems that are difficult with current methods. The methodology also enables systematic categorization of tension member integration patterns: perimeter tension with central compression, alternating horizontal layers, helical tension paths through vertical compression, or radial tension-compression networks. Research priorities include developing automated algorithms for identifying optimal merge candidates using geometric similarity metrics and establishing performance criteria that balance structural performance with fabrication complexity.

#### References

Akbarzadeh, M. (2016). 3D Graphic Statics Using Reciprocal Polyhedral Diagrams. Ph.D. thesis, ETH Zurich, Zurich, Switzerland.

Akbarzadeh, M., Hablicsek, M. (2020). Geometric degrees of freedom and non-conventional spatial structural forms, in: C. Gengnagel, O. Baverel, J. Burry, M. Ramsgaard Thomsen, S. Weinzierl (Eds.), Impact: Design With All Senses, Springer International Publishing, Cham, 3–17.

Akbarzadeh, M. Hablicsek, M. (2021). Algebraic 3d graphic statics: Constrained areas. Computer-Aided Design, 141.

Alic, V., Åkesson, D. (2017). Bi-directional algebraic graphic statics. Computer-Aided Design, 93, 26-37.

Culmann, K. (1864). Die Graphische Statik. Verlag Meyer und Zeller, Zurich, Switzerland.

Hablicsek, M., Akbarzadeh, M., Guo, Y. (2019). Algebraic 3d graphic statics: Reciprocal constructions. Computer-Aided Design, 108, 30-41.

- Lu, Y., Hablicsek, M., Akbarzadeh, M. (2024). Algebraic 3D graphic statics with edge and vertex constraints: A comprehensive approach to extend the solution space for polyhedral form-finding. Computer-Aided Design, 166.
- Maxwell, J. C. (1864). XLV. on reciprocal figures and diagrams of Forces. The London, Edinburgh, and Dublin Philosophical Magazine and Journal of Science, 27(182), 250-261.
- Micheletti, A. (2008). On generalized reciprocal diagrams for self-stressed frameworks. International Journal of Space Structures, 135-166.

Nejur, A., Akbarzadeh, M. (2021). Polyframe, efficient computation for 3d graphic statics. Computer-Aided Design, 134.

Rankine, W. J. M. (1864). Principle of the Equilibrium of Polyhedral Frame. Philosophical Magazine Series 4 27 (1864) 92.

Van Mele, T., Block, P. (2014). Algebraic graph statics. Computer-Aided Design, 53, 104-116.